Am J Transl Res 2026;18(4):3640-3653
www.ajtr.org /ISSN:1943-8141/AJTR0172076

Original Article

Genetically prioritized plasma proteins in intracerebral hemorrhage identified by Mendelian randomization with functional evidence of neuronal vulnerability

Heng Gu[1*], Yan-Song Bu[2*], Jing-Jing Niu[3*], Hui-Min Zhao[1*], Jia-He Li[4*], Xiao-Tong Jiang[4*], Shu-Tong Wu[5*], Guo-Li Xu[6*], Shuai Yu[1], Hong-Xuan Feng[1], Fan-Zhen Kong[4], Guan-Hui Wu[1,2]

[1]Department of Neurology, The Affiliated Suzhou Hospital of Nanjing Medical University, Suzhou Municipal Hospital, Suzhou 215002, Jiangsu, China; [2]Department of Rehabilitation Medicine, Suzhou Municipal Hospital Rehabilitation Medical Center, Dalian Medical University School of Health-Preservation and Wellness, Suzhou 215000, Jiangsu, China; [3]Linyi Central Hospital, Linyi 250000, Shandong, China; [4]Department of Psychology, Suzhou Guangji Hospital, Affiliated Guangji Hospital of Soochow University, Suzhou Mental Health Center, Suzhou 215031, Jiangsu, China; [5]International Department of Suzhou No. 1 High School of Jiangsu Province, Suzhou 215000, Jiangsu, China; [6]Department of Neurology, Suzhou Ninth People's Hospital, Suzhou 215200, Jiangsu, China. [*]Equal contributors.

Received February 12, 2026; Accepted March 23, 2026; Epub April 25, 2026; Published April 30, 2026

Abstract: Objectives: Our study aims to assess the causal association between plasma proteins, immune cell phenotypes and intracerebral hemorrhage (ICH) and explore their downstream biological correlation. Methods: We adopted the two-sample Mendelian randomization (MR) approach. The analysis evaluated the effects of more than 4,000 plasma proteins and 731 immune cell phenotypes on the risk of ICH. Bidirectional MR, mediation effect and sensitivity analysis confirm the causal relationship. We transfect SH-SY5Y neuroblastoma cells and overexpress AHSP or ITGB5 to observe possible function effects. Results: MR analysis linked 299 plasma proteins with ICH ($P < 0.05$), of which 60 proteins showed strong statistical support ($P < 0.01$) and there was no reverse causality. Eighteen types of immune cells also affect ICH risk. Mediation analysis identified 6 causal axes to link specific proteins (IGF1R, NT5E/CD73, ITGB5, CUZD1, and AHSP) with ICH, in which different B cell and T cell subgroups play a key intermediary role. Overexpression of AHSP or ITGB5 inhibits the proliferation and migration of SH-SY5Y cells while promoting their apoptosis. Conclusions: We combined genetics and laboratory data to find that several plasma proteins affect ICH risk. The immune pathway seems to link these proteins with ICH. Although we acknowledge the limitations of MR analysis and in vitro experimental frameworks, the apoptosis promoting effects of AHSP and ITGB5 provide preliminary functional evidence of their role in neuronal damage. Targeting these pathways may provide new strategies for intervention in ICH.

Keywords: Intracerebral hemorrhage, Mendelian randomization, plasma proteins, immune cell phenotypes, IGF1R, AHSP, ITGB5

Introduction

As a critical stroke subtype, intracerebral hemorrhage (ICH) can lead to rapid deterioration of nerve function and high early mortality [1-4]. Despite progress in intensive care, many survivors still face permanent disabilities, and the global burden of the disease continues to increase. At present, there is still a lack of effective treatment plans that can change the clinical process of ICH [1, 5]. Existing evidence shows that the pathological mechanism of ICH is not a simple rupture of blood vessels. It involves the multifaceted interaction between circulating protein, immune activation and specific nerve damage cascade responses during the progression of the disease [6, 7]. These processes may jointly affect brain damage after bleeding. Although, the factors that increase individual susceptibility to ICH are still not fully clear. The biological links between plasma protein imbalance and hemorrhagic brain injury also remain poorly understood. A clearer view of these mechanisms is needed. Identifying

https://doi.org/10.62347/TBCS8286

upstream molecular drivers may help reveal useful biomarkers and potential therapeutic targets for early prevention, risk assessment, and more precise clinical intervention.

High-throughput plasma proteomics and genome-wide Mendelian randomization (MR) have become useful tools for studying complex diseases. These approaches help identify potential causal factors. They can also detect protein mediators that are less affected by environmental confounding factors [8, 9]. Parallel advances in immune cell phenotyping have uncovered substantial heterogeneity within B cell, T cell, and dendritic cell subsets. These immune cells play key roles in neuroinflammation and post-stroke secondary injury [10-12]. Prior studies have reported immune activation after ischemic stroke. But the causal immune mechanisms specific to ICH remain poorly understood. Integrative MR analysis links plasma proteins, immune phenotypes, and ICH risk. This strategy helps identify upstream protein signals and downstream immune mediators and reveal biological pathways that influence susceptibility to hemorrhagic brain injury. Such multi-layer causal frameworks have not yet been systematically established.

By integrating large-scale two-sample MR with immune-mediated analysis and neuronal functional assays, we investigated the pathogenic interplay between plasma proteins, immune phenotypes, and neuronal vulnerability in ICH. Our experimental data reveal that AHSP and ITGB5 actively inhibit neuronal proliferation and migration while inducing apoptosis. Our research has established a key link between circulating protein, immune disorders and nerve damage. It provides new insights into the molecular mechanism of ICH and identifies potential therapeutic targets.

Materials and methods

Study design

We evaluated the relationship between plasma proteins, immune cell phenotypes, and ICH by integrating two-sample MR and mediation analysis. Genetic instrumental variables (IVs) were strictly filtered based on the three core assumptions: strong correlation with the exposure, independence from confounding factors, and exclusivity in affecting the outcome solely through the exposure [13]. Upon establishing a significant causal link, we performed mediation MR to determine whether immune cell phenotypes act as intermediate factors between plasma proteins and ICH risk. These bioinformatic predictions were validated through functional assays (colony formation assay, Transwell migration assay, and terminal deoxynucleotidyl transferase dUTP nick-end labeling (TUNEL) assay) in neuronal cell lines. **Figure 1** outlines this entire workflow.

Data source

Plasma protein data were derived from the Icelandic cohort reported by Ferkingstad et al. [14], which includes pQTL information for 4,907 proteins measured in 35,559 individuals. Immune phenotype data were obtained from the genome-wide association study (GWAS) study by Orrù et al. [15]. The Sardinian cohort provides summary statistics for a wide range of immune cell traits (GCST0001391-GCST0002121) based on 3,757 participants. Genetic data for ICH were downloaded from the IEU Open GWAS database (ebi-a-GCST90018870; https://gwas.mrcieu.ac.uk/). This dataset includes 1,935 cases and 471,578 controls of European ancestry and covers 24,191,284 SNPs.

Genetic instrument selection

We first extracted single nucleotide polymorphisms (SNPs) highly related to the exposure ($P < 1 \times 10^{-5}$) as candidate IVs. Next, we removed SNPs that were in linkage disequilibrium and retained independent IVs ($r^2 = 0.001$, kb = 10,000). Additionally, we ensured consistency in the effect size and alleles of the SNPs between the exposure and outcome datasets, excluding SNPs with a minor allele frequency (MAF) less than 0.01. To prevent weak instrument bias, we measured IV strength using the equation $F = (N - K - 1) \times R^2/(K \times (1 - R^2))$. N denotes sample size, K is the SNPs count, R^2 indicates the cumulative explained variance of the selected SNPs. Any instrument with an F value below 10 was removed.

MR analysis

Causal relationships were primarily estimated using inverse variance weighting (IVW) [16], supported by MR-Egger, weighted median, sim-

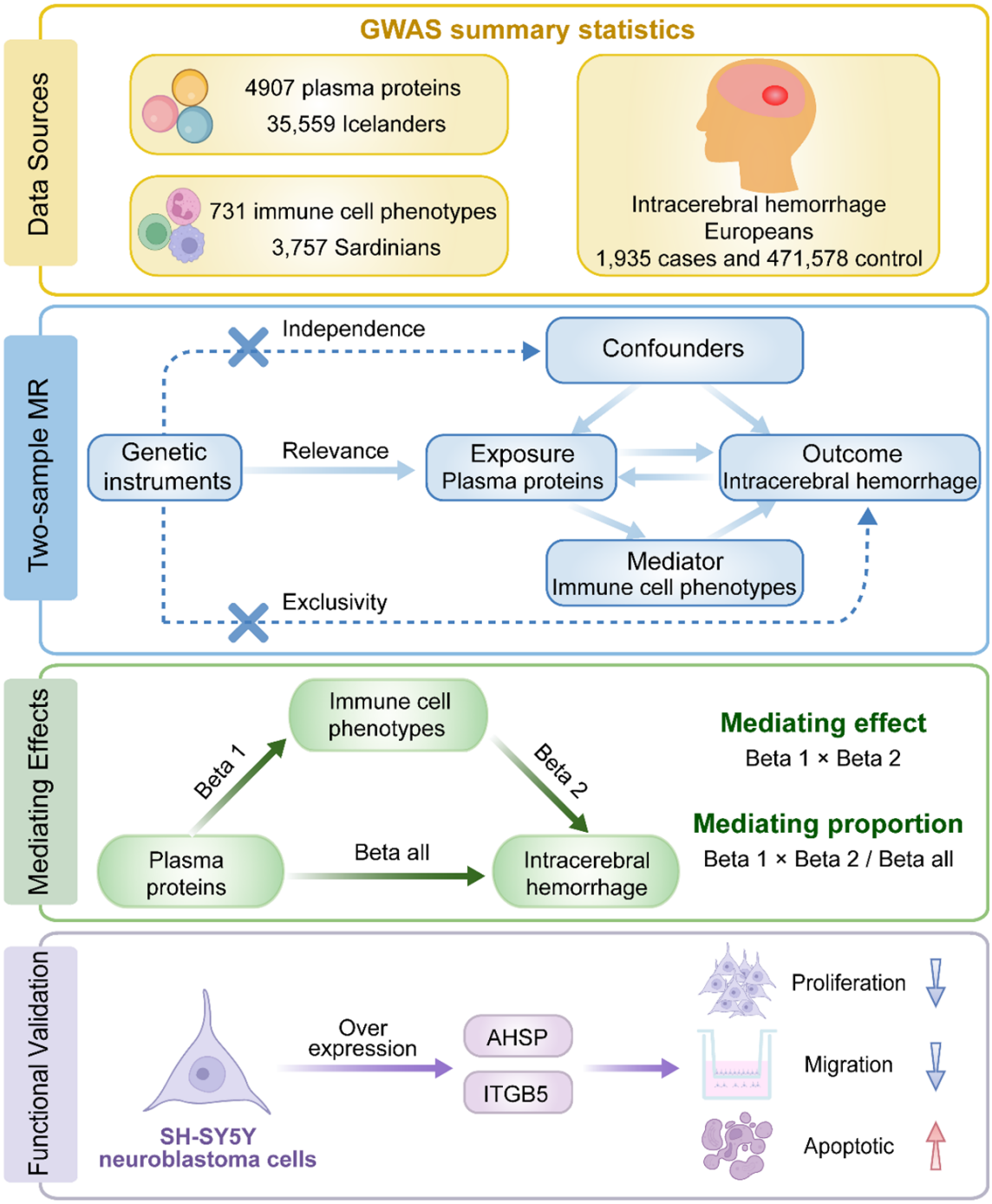

Figure 1. The overall study design and experimental workflow.

ple mode, and weighted mode. First, our two-sample MR evaluated whether plasma proteins and immune cell phenotypes drive ICH risk. A reverse MR (setting plasma proteins as the outcome, ICH as the exposure) was performed to eliminate reverse causality. After the initial MR analysis, significant plasma proteins and immune cell phenotypes were selected for further analysis. Second-step analysis was used to examine whether immune cell phenotypes mediate the protein-ICH pathway. The causal effect between ICH-related proteins and ICH-related immune cell phenotypes were investigated. To measure this mediation, we applied the product-of-coefficients formula. Mediation proportion was obtained by dividing

the indirect effect (Beta 1 × Beta 2) by the total effect (Beta all). Beta 1 defines the protein's influence on immune cell phenotypes, Beta 2 captures the immune cell phenotypes's impact on ICH, and Beta all corresponds to the overall effect of proteins on ICH.

Cell culture

Human SH-SY5Y neuroblastoma cells were cultured in DMEM/F12 medium (Gibco) containing 10% fetal bovine serum (FBS) and 1% penicillin-streptomycin. The cells grew in a 37°C incubator with 5% CO_2 and were passaged at 70-80% confluence.

Plasmid constructs and transfection

Full-length cDNA sequences of human AHSP and ITGB5 were inserted into the pcDNA3.1(+) vector containing a C-terminal Flag epitope. The empty vector (EV) acted as negative control. Flag-AHSP or Flag-ITGB5 plasmids were introduced into SH-SY5Y cells via transfection using Lipofectamine 3000 (Invitrogen) as previously described [17, 18]. Protein expression was assessed 48 hours after transfection.

Immunoblotting

For protein analysis, we lysed cells in RIPA buffer with protease inhibitors and determined concentrations via a BCA kit. We resolved equal protein amounts using SDS-PAGE, followed by a transfer to PVDF membranes. The blots were incubated at 4°C with primary antibodies (anti-Flag, Sigma; anti-β-tubulin, Proteintech) after a 5% skim milk blocking step. Finally, we washed the membranes, added HRP-conjugated secondary antibodies for an hour at room temperature, and captured the chemiluminescent signals [19, 20].

Colony formation assay

To evaluate proliferative ability, we cultured transfected SH-SY5Y cells in 6-well plates (500-1,000 cells/well). After 14 days of culture, we fixed the obtained colony with 4% polyformaldehyde for 20 minutes, and then dyed it with 0.1% crystal violet as detailed previously [21, 22].

Transwell migration assay

Transfected SH-SY5Y cells (5×10^4) were inoculated in the upper chamber of the Transwell chamber (8 μm aperture, Corning) and cultured with serum-free culture medium to evaluate their migration ability [23, 24]. The chemoattractant culture medium containing FBS was added to the lower chamber. After incubation, the cells were fixed and stained with crystal violet. Quantitative analysis was performed on cells that migrated to the lower membrane surface.

TUNEL assay

We applied TUNEL Fluorescence Detection Kit (Vazyme) to detect transfected cells to evaluate cell apoptosis [25, 26]. Cells were fixed with 4% paraformaldehyde and permeabilized with 0.1% Triton X-100, and then incubated with TUNEL reagent at 37°C for an hour. The nuclei were re-stained with DAPI, and the images were collected by a confocal microscope.

Statistical and sensitivity analysis

Statistical work was completed in R (version 4.3.1) using packages such as "TwoSampleMR", "MendelianRandomization", and "MR-PRESSO" (Mendelian Randomization Pleiotropy RESidual Sum and Outlier). We have conducted a number of sensitivity analyses to detect the deviations that may be caused by pleiotropy or heterogeneity. We evaluated horizontal pleiotropy using MR-Egger intercepts, and regarded $P > 0.05$ as an indicator of no pleiotropy. MR-PRESSO global test further helped us identify and eliminate abnormal SNPs to prevent deviations from the estimated value. To check for heterogeneity among the genetic instruments, we calculated Cochran's Q statistic ($P > 0.05$ shows no heterogeneity). No single variation affecting the final causal result was confirmed using the leave-one-out approach. All assays were conducted with at least three independent replicates. Quantitative results are reported as mean ± standard deviation (SD). Comparisons adopted two-tailed Student's t-test or one-way ANOVA with appropriate post-hoc tests. Differences were considered significant when $P < 0.05$.

Results

Causal link between plasma proteins and intracerebral hemorrhage

We first screened for causal links from plasma proteins to ICH using a two-sample MR

approach. IVW estimates identified 299 proteins influencing ICH risk (P < 0.05). Among them, 60 proteins demonstrated robust associations (P < 0.01) (**Table 1**). Of these, 40 plasma proteins were linked to a higher likelihood of ICH (odds ratios [OR] > 1, P_{IVW} < 0.01), while 20 plasma proteins appeared to exert protective effects (OR < 1, P_{IVW} < 0.05). The top 10 risk drivers based on OR values were SPINK13 (OR [95% Confidence Interval (CI)]: 2.793 [1.456-5.360], P = 0.002), KLRC4 (OR [95% CI]: 2.034 [1.292-3.205], P = 0.002), PTS (OR [95% CI]: 1.962 [1.250-3.080], P = 0.003), FSHB (OR [95% CI]: 1.838 [1.339-2.525], P < 0.001), NAGS (OR [95% CI]: 1.788 [1.155-2.769], P = 0.009), BGLAP (OR [95% CI]: 1.731 [1.208-2.479], P = 0.003), PIAS3 (OR [95% CI]: 1.710 [1.230-2.377], P = 0.001), CRMP1 (OR [95% CI]: 1.701 [1.200-2.411], P = 0.003), PATE1 (OR [95% CI]: 1.659 [1.160-2.373], P = 0.006), and ITGB2 (OR [95% CI]: 1.583 [1.147-2.184], P = 0.005). A subsequent reverse MR analysis with 60 plasma proteins as outcome and ICH as the exposure was conducted. The IVW analysis showed no significant reverse causal relationship between ICH and these 60 plasma proteins (P > 0.05) (**Table 1**).

Causal link between plasma proteins and immune cell phenotypes

We also screened 731 immune cell phenotypes for potential causal effects on ICH. The IVW method identified 18 phenotypes that significantly alter ICH risk (P < 0.05) (**Figure 2**; Table S1). Eight of these phenotypes actively increased ICH susceptibility: Side Scatter-Area on CD8bright T cells (SSC-A on CD8br) (OR [95% CI]: 1.178 [1.019-1.360], P = 0.026), CD25 expression on CD39-positive activated regulatory T cells (CD25 on CD39+ activated Treg) (OR [95% CI]: 1.152 [1.002-1.323], P = 0.046), CD45RA expression on terminally differentiated CD8bright T cells (CD45RA on TD CD8br) (OR [95% CI]: 1.145 [1.024-1.280], P = 0.018), absolute count of CD24-positive CD27-positive B cells (CD24+ CD27+ AC) (OR [95% CI]: 1.144 [1.036-1.263], P = 0.008), HLA DR expression on HLA DR-positive CD8bright T cells (HLA DR on HLA DR+ CD8br) (OR [95% CI]: 1.140 [1.015-1.280], P = 0.027), memory B cell percentage of total B cells (Memory B cell %B cell) (OR [95% CI]: 1.114 [1.000-1.241], P = 0.050), unswitched memory B cell percentage of total B cells (Unsw mem %B cell) (OR [95% CI]: 1.095 [1.009-1.189], P = 0.030), and CD39 expression on CD39-positive CD4-positive T cells (CD39 on CD39+ CD4+) (OR [95% CI]: 1.086 [1.013-1.163], P = 0.019).

In contrast, ten immune cell phenotypes were linked to a reduced risk of ICH: HLA DR expression on dendritic cells (HLA DR on DC) (OR [95% CI]: 0.953 [0.911-0.997], P = 0.036), BAFF-receptor expression on IgD-positive CD24-negative B cells (BAFF-R on IgD+ CD24-) (OR [95% CI]: 0.947 [0.899-0.998], P = 0.044), CD3 expression on CD28-positive CD45RA-positive CD8bright T cells (CD3 on CD28+ CD45RA+ CD8br) (OR [95% CI]: 0.934 [0.875-0.998], P = 0.044), CD27 expression on switched memory B cells (CD27 on sw mem) (OR [95% CI]: 0.929 [0.875-0.987], P = 0.017), absolute count of CD25-highly-positive CD8bright T cells (CD25++ CD8br AC) (OR [95% CI]: 0.920 [0.856-0.988], P = 0.023), absolute count of CD33-negative HLA DR-positive cells (CD33- HLA DR+ AC) (OR [95% CI]: 0.909 [0.842-0.982], P = 0.015), naive CD4-positive T cell percentage of total T cells (Naive CD4+ %T cell) (OR [95% CI]: 0.895 [0.823-0.973], P = 0.009), absolute count of CD28-negative CD8-dim T cells (CD28- CD8dim AC) (OR [95% CI]: 0.892 [0.822-0.967], P = 0.006), transitional B cell percentage of total B cells (Transitional %B cell) (OR [95% CI]: 0.879 [0.790-0.979], P = 0.019), and CD39-positive activated regulatory T cell percentage of total activated regulatory T cells (CD39+ activated Treg %activated Treg) (OR [95% CI]: 0.791 [0.662-0.946], P = 0.010).

Mediation effect of immune cell phenotypes on plasma protein-driven intracerebral hemorrhage

After identifying proteins associated with ICH, we further examined whether immune phenotypes mediate these effects. Next, we explored the impact of 60 ICH-related plasma proteins on 18 ICH-related immune cell phenotypes. After ensuring the logical consistency of effect size directions, we identified 6 plasma protein-immune cell phenotypes-ICH causal pathways, involving 5 plasma proteins and 6 immune cell phenotypes (**Figure 3**). Specifically, CD24+ CD27+ AC and Unsw mem %B cells may mediate the association between IGF1R and ICH, with mediation proportions of 17.5% and 10.8%, respectively; Transitional %B cell may mediate the effect of NT5E on ICH, with a medi-

Table 1. Causal link between plasma proteins and intracerebral hemorrhage (ICH)

Exposure	Outcome	OR (95% CI)	Pval	revPval
SPINK13	Intracerebral hemorrhage	2.793 (1.456, 5.360)	0.002	0.518
KLRC4	Intracerebral hemorrhage	2.034 (1.292, 3.205)	0.002	0.523
PTS	Intracerebral hemorrhage	1.962 (1.250, 3.080)	0.003	0.264
FSHB	Intracerebral hemorrhage	1.838 (1.339, 2.525)	< 0.001	0.837
NAGS	Intracerebral hemorrhage	1.788 (1.155, 2.769)	0.009	0.349
BGLAP	Intracerebral hemorrhage	1.731 (1.208, 2.479)	0.003	0.794
PIAS3	Intracerebral hemorrhage	1.710 (1.230, 2.377)	0.001	0.677
CRMP1	Intracerebral hemorrhage	1.701 (1.200, 2.411)	0.003	0.777
PATE1	Intracerebral hemorrhage	1.659 (1.160, 2.373)	0.006	0.799
ITGB2	Intracerebral hemorrhage	1.583 (1.147, 2.184)	0.005	0.944
AGA	Intracerebral hemorrhage	1.571 (1.154, 2.140)	0.004	0.576
CPLX1	Intracerebral hemorrhage	1.554 (1.116, 2.164)	0.009	0.949
ALDOB	Intracerebral hemorrhage	1.550 (1.145, 2.098)	0.005	0.856
CUBN	Intracerebral hemorrhage	1.546 (1.115, 2.146)	0.009	0.529
TNFRSF4	Intracerebral hemorrhage	1.536 (1.118, 2.110)	0.008	0.750
B3GALT6	Intracerebral hemorrhage	1.533 (1.197, 1.964)	< 0.001	0.828
ETV5	Intracerebral hemorrhage	1.521 (1.111, 2.083)	0.009	0.608
IL24	Intracerebral hemorrhage	1.515 (1.107, 2.073)	0.010	0.746
CUZD1	Intracerebral hemorrhage	1.480 (1.160, 1.889)	0.002	0.459
ANXA8	Intracerebral hemorrhage	1.470 (1.122, 1.926)	0.005	0.914
CD79B	Intracerebral hemorrhage	1.466 (1.116, 1.927)	0.006	0.981
S100A6	Intracerebral hemorrhage	1.438 (1.111, 1.860)	0.006	0.507
FBP1	Intracerebral hemorrhage	1.425 (1.109, 1.832)	0.006	0.866
IDH1	Intracerebral hemorrhage	1.408 (1.096, 1.807)	0.007	0.523
ITGB5	Intracerebral hemorrhage	1.405 (1.121, 1.762)	0.003	0.816
AHSP	Intracerebral hemorrhage	1.397 (1.148, 1.700)	< 0.001	0.858
PRKCG	Intracerebral hemorrhage	1.389 (1.098, 1.758)	0.006	0.483
RBP7	Intracerebral hemorrhage	1.385 (1.150, 1.669)	< 0.001	0.189
TNFRSF1B	Intracerebral hemorrhage	1.310 (1.090, 1.574)	0.004	0.228
TNFSF18	Intracerebral hemorrhage	1.299 (1.089, 1.551)	0.004	0.900
EXTL2	Intracerebral hemorrhage	1.291 (1.071, 1.556)	0.007	0.822
TRADD	Intracerebral hemorrhage	1.261 (1.065, 1.494)	0.007	0.681
ACAA1	Intracerebral hemorrhage	1.246 (1.056, 1.471)	0.009	0.859
CRIPT	Intracerebral hemorrhage	1.232 (1.064, 1.427)	0.005	0.266
IGF1R	Intracerebral hemorrhage	1.228 (1.070, 1.409)	0.003	0.930
PRSS1	Intracerebral hemorrhage	1.223 (1.061, 1.411)	0.006	0.656
A4GALT	Intracerebral hemorrhage	1.195 (1.059, 1.348)	0.004	0.631
PLXNB2	Intracerebral hemorrhage	1.175 (1.042, 1.325)	0.009	0.656
NT5E	Intracerebral hemorrhage	1.145 (1.038, 1.264)	0.007	0.067
THSD1	Intracerebral hemorrhage	1.138 (1.036, 1.250)	0.007	0.895
GPC1	Intracerebral hemorrhage	0.863 (0.778, 0.958)	0.006	0.220
CRP	Intracerebral hemorrhage	0.815 (0.714, 0.931)	0.003	0.721
NMRAL1	Intracerebral hemorrhage	0.809 (0.696, 0.941)	0.006	0.793
ANXA4	Intracerebral hemorrhage	0.792 (0.666, 0.943)	0.009	0.477
SPOCK2	Intracerebral hemorrhage	0.778 (0.669, 0.905)	0.001	0.801
PPIL1	Intracerebral hemorrhage	0.771 (0.639, 0.929)	0.006	0.949
UBE2E1	Intracerebral hemorrhage	0.740 (0.606, 0.905)	0.003	0.899

SUMO3	Intracerebral hemorrhage	0.711 (0.557, 0.909)	0.006	0.910
AIF1	Intracerebral hemorrhage	0.704 (0.539, 0.918)	0.010	0.767
KLK3	Intracerebral hemorrhage	0.691 (0.530, 0.902)	0.006	0.608
CACYBP	Intracerebral hemorrhage	0.690 (0.531, 0.896)	0.005	0.872
TBCB	Intracerebral hemorrhage	0.676 (0.504, 0.907)	0.009	0.693
TBCE	Intracerebral hemorrhage	0.667 (0.490, 0.906)	0.010	0.655
AXIN2	Intracerebral hemorrhage	0.665 (0.534, 0.829)	< 0.001	0.397
ICAM5	Intracerebral hemorrhage	0.660 (0.523, 0.835)	< 0.001	0.134
GNPNAT1	Intracerebral hemorrhage	0.660 (0.483, 0.902)	0.009	0.612
PGR	Intracerebral hemorrhage	0.659 (0.490, 0.886)	0.006	0.876
CILP	Intracerebral hemorrhage	0.658 (0.479, 0.904)	0.010	0.815
BID	Intracerebral hemorrhage	0.645 (0.491, 0.845)	0.001	0.883
AGFG1	Intracerebral hemorrhage	0.548 (0.361, 0.831)	0.005	0.755

revPval: The *P* value of reverse mendelian randomization (MR) analysis.

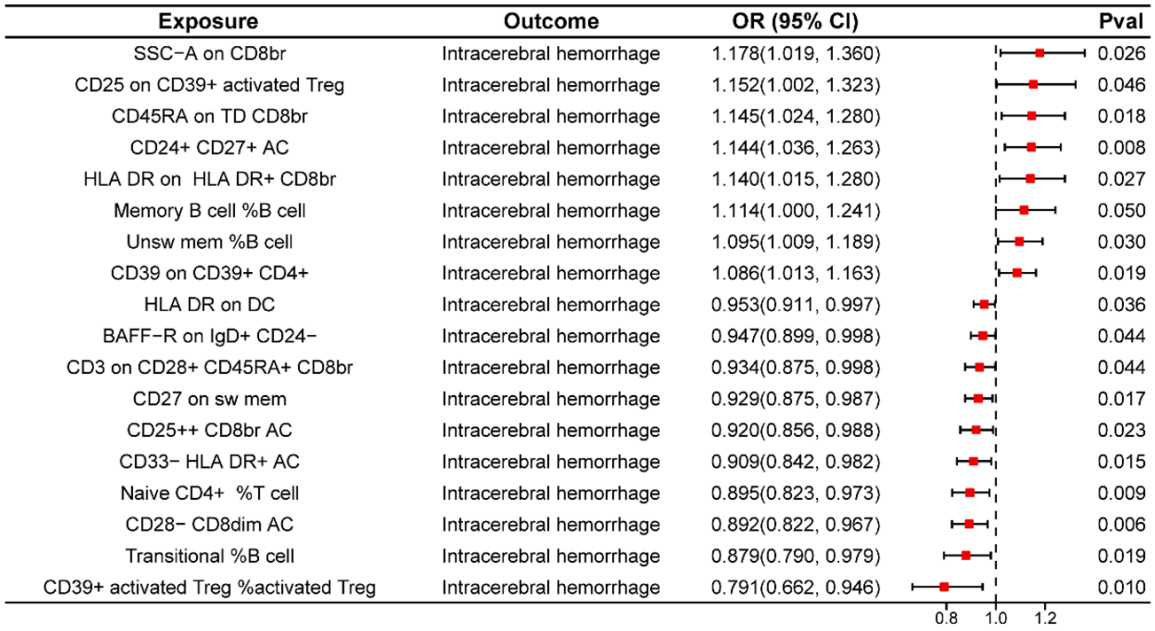

Figure 2. Forest plot of causal associations between immune cell phenotypes and intracerebral hemorrhage (ICH). Mendelian randomization (MR) analysis identified 18 immune cell phenotypes that are significantly causally associated with ICH ($P_{IVW} < 0.05$).

ation proportion of 14%; SSC-A on CD8br may mediate the influence of ITGB5 on ICH, with a mediation proportion of 9.92%; CD28- CD8dim AC may mediate the association between CUZD1 and ICH, with a mediation proportion of 8.06%; and CD39 on CD39+ CD4+ may mediate the relationship between AHSP and ICH, accounting for 4.97% of the total effect (**Table 2**).

These results indicate that IGF1R may elevate ICH risk by increasing the levels of CD24+ CD27+ AC or Unsw mem %B cells, NT5E may increase ICH risk by reducing transitional %B cells, ITGB5 may increase ICH risk by increasing SSC-A on CD8br, CUZD1 may increase ICH risk by reducing CD28- CD8dim AC, and AHSP may increase ICH risk by increasing CD39 on CD39+ CD4+ (**Figure 3**).

To verify these findings, we ran multiple sensitivity checks (**Table 3**). Cochran's Q statistics confirmed uniform SNP effects across the board, safely ruling out heterogeneity (all P >

Exposure	Outcome	nSNP	Method	Pval	OR(95% CI)
IGF1R	CD24+ CD27+ AC	24	IVW	<0.001	1.306 (1.118 to 1.526)
CD24+ CD27+ AC	Intracerebral hemorrhage	22	IVW	0.0077	1.144 (1.036 to 1.263)
IGF1R	Intracerebral hemorrhage	25	IVW	0.0035	1.228 (1.070 to 1.409)
IGF1R	Unsw mem %B cell	24	IVW	0.0024	1.276 (1.090 to 1.493)
Unsw mem %B cell	Intracerebral hemorrhage	27	IVW	0.0305	1.095 (1.009 to 1.189)
IGF1R	Intracerebral hemorrhage	25	IVW	0.0035	1.228 (1.070 to 1.409)
NT5E	Transitional %B cell	47	IVW	0.0047	0.862 (0.778 to 0.956)
Transitional %B cell	Intracerebral hemorrhage	15	IVW	0.0191	0.879 (0.790 to 0.979)
NT5E	Intracerebral hemorrhage	53	IVW	0.0071	1.145 (1.038 to 1.264)
ITGB5	SSC−A on CD8br	26	IVW	0.0439	1.229 (1.006 to 1.503)
SSC−A on CD8br	Intracerebral hemorrhage	13	IVW	0.0264	1.178 (1.019 to 1.360)
ITGB5	Intracerebral hemorrhage	28	IVW	0.0032	1.405 (1.121 to 1.762)
CUZD1	CD28− CD8dim AC	19	IVW	0.0328	0.759 (0.589 to 0.978)
CD28− CD8dim AC	Intracerebral hemorrhage	23	IVW	0.0056	0.892 (0.822 to 0.967)
CUZD1	Intracerebral hemorrhage	19	IVW	0.0016	1.480 (1.160 to 1.889)
AHSP	CD39 on CD39+ CD4+	28	IVW	0.0291	1.224 (1.021 to 1.467)
CD39 on CD39+ CD4+	Intracerebral hemorrhage	21	IVW	0.0193	1.086 (1.013 to 1.163)
AHSP	Intracerebral hemorrhage	28	IVW	<0.001	1.397 (1.148 to 1.700)

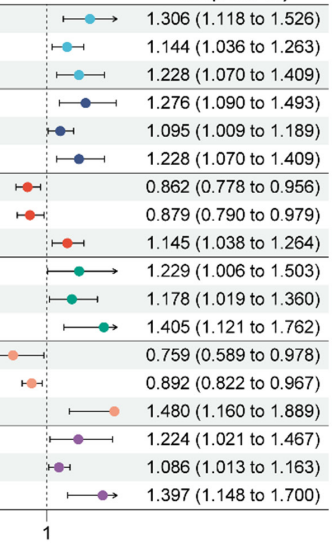

Figure 3. Forest plot of causal associations between plasma proteins, immune cell phenotypes and ICH. MR analysis revealed 6 significant causal pathways involving 5 plasma proteins and 6 immune cell phenotypes associated with ICH.

Table 2. Mediation effect of immune cell phenotypes on plasma protein-driven ICH

Plasma proteins	Immune cell phenotypes	Outcome	Beta all	Mediated effect	Mediated proportion
IGF1R	CD24+ CD27+ AC	Intracerebral hemorrhage	0.205	0.036 (-0.011, 0.083)	17.50%
IGF1R	Unsw mem %B cell	Intracerebral hemorrhage	0.205	0.022 (-0.019, 0.063)	10.80%
NT5E	Transitional %B cell	Intracerebral hemorrhage	0.136	0.019 (-0.001, 0.039)	14%
ITGB5	SSC-A on CD8br	Intracerebral hemorrhage	0.340	0.034 (-0.019, 0.087)	9.92%
CUZD1	CD28- CD8dim AC	Intracerebral hemorrhage	0.392	0.032 (-0.044, 0.107)	8.06%
AHSP	CD39 on CD39+ CD4+	Intracerebral hemorrhage	0.334	0.017 (-0.023, 0.056)	4.97%

0.05). No significant horizontal pleiotropy was detected, as the MR-Egger intercept was centered around zero (P > 0.05). The causal estimates remained consistent throughout the leave-one-out evaluations (Figures S1, S2, S3). Together, these results support the robustness of the identified protein-immune cell-ICH pathways.

AHSP and ITGB5 suppress proliferation and migration while inducing apoptosis in SH-SY5Y cells

Given the immune cell mediation identified via MR analysis, the human neuroblastoma cell line SH-SY5Y was utilized as a simplified in vitro neuronal-like model to explore the potential cellular effects of AHSP and ITGB5. To achieve ectopic expression, we transfected SH-SY5Y cells with Flag-tagged AHSP, ITGB5, or an EV control. Immunoblotting showed clear bands at the expected molecular weight, while the EV control group did not resolve a detectable exogenous protein signal, confirming the significant overexpression of AHSP-Flag and ITGB5-Flag (**Figure 4A**).

We employed a colony formation assay to determine cell proliferation. AHSP or ITGB5 overexpression significantly suppressed cell proliferation (**Figure 4B**, **4C**). Transwell assay exhibited that AHSP or ITGB5 overexpression reduced the number of migrated cells, with sparse and scattered staining on the membrane (**Figure 4D**, **4E**). To further assess cell death, TUNEL staining was performed in SH-SY5Y cells to determine whether AHSP or ITGB5 overexpression affects apoptosis. Compared with the EV group, which exhibited only sparse TUNEL-positive nuclei, both AHSP- and

Table 3. The heterogeneity and pleiotropy in MR analysis

Exposure	Outcome	Heterogeneity test				Pleiotropy test		
		IVW		MR Egger		MR Egger regression		
		Cochran Q	Pval	Cochran Q	Pval	Intercept	se	Pval
IGF1R	CD24+ CD27+ AC	16.190	0.847	16.189	0.806	0.001	0.013	0.968
CD24+ CD27+ AC	Intracerebral hemorrhage	20.434	0.494	19.017	0.521	-0.023	0.019	0.248
IGF1R	Unsw mem %B cell	13.612	0.937	13.007	0.933	0.010	0.013	0.445
Unsw mem %B cell	Intracerebral hemorrhage	28.185	0.349	28.181	0.300	-0.001	0.016	0.951
IGF1R	Intracerebral hemorrhage	19.986	0.698	19.587	0.667	0.008	0.012	0.534
NT5E	Transitional %B cell	46.680	0.444	46.679	0.403	-0.000	0.008	0.983
Transitional %B cell	Intracerebral hemorrhage	9.440	0.802	8.775	0.790	0.020	0.024	0.430
NT5E	Intracerebral hemorrhage	60.275	0.201	60.072	0.180	-0.003	0.008	0.680
ITGB5	SSC-A on CD8br	21.949	0.639	21.844	0.589	0.005	0.016	0.749
SSC-A on CD8br	Intracerebral hemorrhage	9.507	0.659	8.904	0.631	-0.027	0.034	0.454
ITGB5	Intracerebral hemorrhage	26.487	0.492	25.188	0.508	-0.020	0.018	0.265
CUZD1	CD28- CD8dim AC	11.417	0.876	11.094	0.852	0.013	0.023	0.577
CD28- CD8dim AC	Intracerebral hemorrhage	20.107	0.576	19.261	0.568	-0.018	0.019	0.368
CUZD1	Intracerebral hemorrhage	19.264	0.376	19.255	0.314	-0.002	0.023	0.928
AHSP	CD39 on CD39+ CD4+	26.849	0.472	25.657	0.482	0.015	0.014	0.285
CD39 on CD39+ CD4+	Intracerebral hemorrhage	13.261	0.866	13.027	0.837	-0.010	0.020	0.635
AHSP	Intracerebral hemorrhage	35.856	0.118	33.373	0.152	0.021	0.015	0.176

ITGB5-overexpressing cells displayed a markedly increased number of apoptotic cells. The intensity and abundance of green TUNEL fluorescence were substantially elevated in both overexpression groups, indicating enhanced DNA fragmentation (**Figure 4F**, **4G**).

Discussion

Based on large-scale genomic datasets, we applied a two-sample MR analysis. The goal was to investigate the causal role of circulating plasma proteins in ICH. A total of 299 proteins showed associations with ICH risk, among which 60 exhibited the strongest causal estimates. Reverse MR analyses also revealed no evidence supporting a causal influence of ICH on circulating protein concentrations [27, 28]. Our analysis identified IGF1R, CUZD1, and AHSP as potential risk-enhancing proteins. Their effects appear to act through specific immune cell subpopulations. These findings expand the list of potential biomarkers related to ICH. They also provide useful clues for future studies that aim to develop protein-based therapeutic strategies for stroke.

We also identified several immune-cell phenotypes that exhibited causal effects on ICH risk. This finding supports the central role of immune responses in secondary injury after stroke. Prior evidence has shown that peripheral immune populations - including B cells, T cells, and monocytes - become strongly activated after ischemic stroke. Their activation can shape the course of neuroinflammation [29-31]. Our study extends earlier findings to hemorrhagic stroke. The analysis identified several immune signatures related to ICH. We found that B and T cell subgroups such as CD24+ CD27+ B cells and CD45RA on TD CD8br T cells are significantly correlated with the risk of disease. Our data is consistent with the established evidence that B cells and Treg cells are involved in the pathogenesis of stroke [11, 32]. Mo et al. also used MR analysis to find causal links between several circulating immune traits and ICH risk, including naive B cells and plasmacytoid dendritic cells [33]. In addition, we also found a protective subgroup, indicating that the increase in HLA-DR+ dendritic cell count is associated with a reduced risk of ICH. Immune mediators may play different roles in different situations. Such dual effects have also been noted in studies of stroke progression.

This study establishes a mediation framework linking plasma protein, immune cell phenotype and ICH. Several proteins including IGF1R,

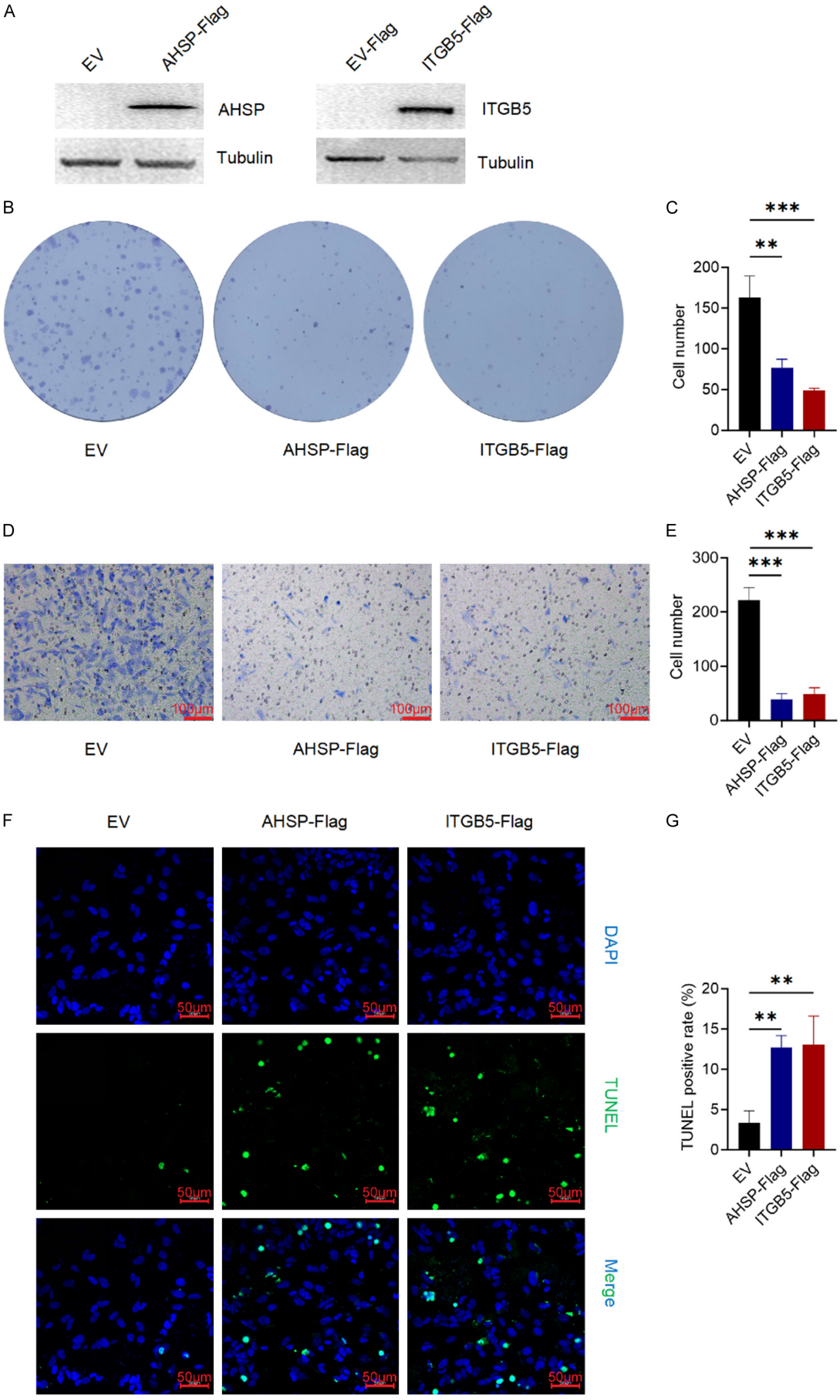
A
EV
AHSP-Flag
EV-Flag
ITGB5-Flag
AHSP
ITGB5
Tubulin
Tubulin
B
EV
AHSP-Flag
ITGB5-Flag
C
***
**
Cell number
200
150
100
50
0
EV
AHSP-Flag
ITGB5-Flag
D
100μm
EV
AHSP-Flag
ITGB5-Flag
E
***
***
Cell number
300
200
100
0
EV
AHSP-Flag
ITGB5-Flag
F
EV
AHSP-Flag
ITGB5-Flag
DAPI
TUNEL
Merge
50μm
G
**
**
TUNEL positive rate (%)
20
15
10
5
0
EV
AHSP-Flag
ITGB5-Flag

Figure 4. Functional validation of AHSP and ITGB5 in SH-SY5Y neuroblastoma cell. A. Western blot analysis confirmed robust overexpression of Flag-tagged AHSP and ITGB5 in transfected SH-SY5Y neuroblastoma cell. B, C. Colony formation assay to detect the proliferation ability of AHSP and ITGB5 overexpression in SH-SY5Y neuroblastoma cells. D, E. Transwell assay to detect the migration capacity of AHSP and ITGB5 overexpression in SH-SY5Y neuroblastoma cells (200×). F, G. TUNEL assay was performed to assess the induction of apoptosis by AHSP and ITGB5 overexpression in SH-SY5Y neuroblastoma cells (400×). **P < 0.01, ***P < 0.001.

NT5E (CD73), ITGB5, CUZD1, and AHSP may influence ICH risk through their effects on specific immune cell subsets. IGF1R increases ICH risk through boosting unswitched memory B cells and CD24+ CD27+ B cell populations. These findings are consistent with the dual neuroprotective and pro-inflammatory roles previously attributed to IGF-1 signaling [34, 35]. Previous MR studies have also linked IGF-1 levels to stroke pathophysiology [36]. Functional experiments provided preliminary in vitro evidence for two newly implicated proteins. In neuroblastoma cells, overexpression of AHSP and ITGB5 strongly suppressed cell proliferation and migration but induced apoptotic responses. ITGB5, the β5 subunit of the integrin family, heterodimerizes with integrin αV to form αVβ5 [37]. Both ITGB5 and its ligand fibronectin increase after high-glucose exposure in vitro and in vivo. Endothelial-specific knockdown of ITGB5 significantly attenuates high-glucose-induced apoptosis and microvascular rarefaction [38]. Our results extend these observations to neural contexts. AHSP is traditionally known as an erythroid chaperone protein [39]. Overexpression of AHSP showed a clear pro-apoptotic effect in neuronal cells. This may be related to disrupted hemoglobin-handling pathways caused by erythrocyte lysis [40]. Taken together with the MR analysis, these experimental results indicate that AHSP or ITGB5 may participate in neuronal injury processes during ICH.

Our genetic and cellular experiments suggest a mechanistic link between circulating proteins, immune responses, and ICH risk. Proteins including IGF1R, NT5E, ITGB5, CUZD1, and AHSP, together with related immune cell phenotypes, may serve as biomarkers and possible targets for ICH treatment. For example, modulating the IGF-1 signaling, CD73 axis, or specific immune-cell subsets may alter ICH risk. Despite the robust causal estimates, the reliance on genetic proxies rather than direct clinical observation warrants cautious interpretation. Translating bioinformatic predictions into therapeutic strategies requires extensive in vivo modeling and prospective tests to verify the exact mechanism cascade. In addition, although our analysis is limited to European descent to minimize stratification. The inclusion of different subgroups (such as Icelanders and Sardinians) will introduce potential residual deviations, so it is necessary to conduct repeated studies in larger-scale and more homogeneous samples.

Acknowledgements

This work was supported by the Fund for Suzhou Municipal Special Project for Clinical Key Disease Diagnosis and Treatment Technologies (LCZX202318) and Suzhou "Science and Education Promoting Health" Youth Science and Technology Project (KJXW2022075).

Disclosure of conflict of interest

None.

Address correspondence to: Guan-Hui Wu, Department of Neurology, The Affiliated Suzhou Hospital of Nanjing Medical University, Suzhou Municipal Hospital, Suzhou 215002, Jiangsu, China. Tel: +86-18061924176; E-mail: ghwusz26@njmu.edu.cn; Fan-Zhen Kong, Department of Psychology, Suzhou Guangji Hospital, Affiliated Guangji Hospital of Soochow University, Suzhou Mental Health Center, Suzhou 215031, Jiangsu, China. Tel: +86-18914052496; E-mail: kongfanzhen0043@suda.edu.cn

References

[1] Wan G, Gu L, Chen Y, Wang Y, Sun Y, Li Z, Ma W, Bao X and Wang R. From bench to bedside: nanomedicine development for intracerebral hemorrhage - exploring microenvironment, innovation, and translation. J Nanobiotechnology 2025; 23: 567.

[2] Puy L, Parry-Jones AR, Sandset EC, Dowlatshahi D, Ziai W and Cordonnier C. Intracerebral haemorrhage. Nat Rev Dis Primers 2023; 9: 14.

[3] Ye L, Tang X, Zhong J, Li W, Xu T, Xiang C, Gu J, Feng H, Luo Q and Wang G. Unraveling the complex pathophysiology of white matter hem-

orrhage in intracerebral stroke: a single-cell RNA sequencing approach. CNS Neurosci Ther 2024; 30: e14652.
[4] Qin J, Zhou L, Yu L, Ye J, Wang F, Zhou J, Gu Y, Chen G and Chen X. Exosomes derived from HUVECs alleviate ischemia-reperfusion induced inflammation in neural cells by upregulating KLF14 expression. Front Pharmacol 2024; 15: 1365928.
[5] Chen Y, Tang W, Huang X, An Y, Li J, Yuan S, Shan H and Zhang M. Mitophagy in intracerebral hemorrhage: a new target for therapeutic intervention. Neural Regen Res 2024; 19: 316-323.
[6] He KL, Yu X, Xia L, Xie YD, Qi EB, Wan L, Hua XM and Jing CH. A new perspective on the regulation of neuroinflammation in intracerebral hemorrhage: mechanisms of NLRP3 inflammasome activation and therapeutic strategies. Front Immunol 2025; 16: 1526786.
[7] Lin J, Xu Y, Guo P, Chen YJ, Zhou J, Xia M, Tan B, Liu X, Feng H and Chen Y. CCL5/CCR5-mediated peripheral inflammation exacerbates blood-brain barrier disruption after intracerebral hemorrhage in mice. J Transl Med 2023; 21: 196.
[8] Zhang Y, Liang Y, Liu M, Liu L, Li J, Li R, Wu Z, Qiao L and Chen J. Identifying plasma proteins and immunocyte phenotypes as risk factors in rheumatoid arthritis: the role of EPHA3 and CD28(+) CD45RA(+) CD8(br) treg cells. Clin Rheumatol 2025; 44: 3525-3537.
[9] Tang Q, Zhang Y, Zhou T, Guo Z, Hu M, Jin J, Feng B, Cao J, Qiao L and Liang Y. Serum IL-18R1 and its effect on immune cell infiltration in asthma. Am J Transl Res 2025; 17: 2112-2123.
[10] Xiu Y, Wang Y, Wang N, Liu N, Jiang Y, Shi M, Zhou D, Sein TY, Kilgore MD, Katakam PVG, Liu Q, Jin WN, Shi FD, Wang X and Dumont AS. T cell receptor activation contributes to brain damage after intracerebral hemorrhage in mice. J Neuroinflammation 2025; 22: 78.
[11] Wang R, Li H, Ling C, Zhang X, Lu J, Luan W, Zhang J and Shi L. A novel phenotype of B cells associated with enhanced phagocytic capability and chemotactic function after ischemic stroke. Neural Regen Res 2023; 18: 2413-2423.
[12] Zhu L, Shang J, Li Y, Zhang Z, Fu P, Zong Y, Chen S, Wang J, Zhang J, Wang J and Jiang C. Toll-like receptors mediate opposing dendritic cell effects on Treg/Th17 balance in mice with intracerebral hemorrhage. Stroke 2024; 55: 2126-2138.
[13] Wang Y, Zhao X, Wang R, Yang Y, Su R, Ni J, Sun Y, Sun S, Zhou X, Yang Y, Yu Y, Shen Y, Tang S, Xu G, Hou X, Xu L, Xiao J and Tian T. Genetic evidence supporting causality between atopic dermatitis and chronic obstructive pulmonary disease. Int Immunopharmacol 2025; 155: 114602.
[14] Ferkingstad E, Sulem P, Atlason BA, Sveinbjornsson G, Magnusson MI, Styrmisdottir EL, Gunnarsdottir K, Helgason A, Oddsson A, Halldorsson BV, Jensson BO, Zink F, Halldorsson GH, Masson G, Arnadottir GA, Katrinardottir H, Juliusson K, Magnusson MK, Magnusson OT, Fridriksdottir R, Saevarsdottir S, Gudjonsson SA, Stacey SN, Rognvaldsson S, Eiriksdottir T, Olafsdottir TA, Steinthorsdottir V, Tragante V, Ulfarsson MO, Stefansson H, Jonsdottir I, Holm H, Rafnar T, Melsted P, Saemundsdottir J, Norddahl GL, Lund SH, Gudbjartsson DF, Thorsteinsdottir U and Stefansson K. Large-scale integration of the plasma proteome with genetics and disease. Nat Genet 2021; 53: 1712-1721.
[15] Orrù V, Steri M, Sidore C, Marongiu M, Serra V, Olla S, Sole G, Lai S, Dei M, Mulas A, Virdis F, Piras MG, Lobina M, Marongiu M, Pitzalis M, Deidda F, Loizedda A, Onano S, Zoledziewska M, Sawcer S, Devoto M, Gorospe M, Abecasis GR, Floris M, Pala M, Schlessinger D, Fiorillo E and Cucca F. Complex genetic signatures in immune cells underlie autoimmunity and inform therapy. Nat Genet 2020; 52: 1036-1045.
[16] Ding Z, Wu L, Xu T, Zhang C, Liang Y, Li J and Zhuang W. The relationship between metabolites and gout: a Mendelian randomization study. Am J Clin Exp Immunol 2024; 13: 177-186.
[17] Lv J, Wu T, Xue J, Shen C, Gao W, Chen X, Guo Y, Liu M, Yu J, Huang X and Zheng B. ASB1 engages with ELOB to facilitate SQOR ubiquitination and H(2)S homeostasis during spermiogenesis. Redox Biol 2025; 79: 103484.
[18] Yu X, Xu B, Gao T, Fu X, Jiang B, Zhou N, Gao W, Wu T, Shen C, Huang X, Wu Y and Zheng B. E3 ubiquitin ligase RNF187 promotes growth of spermatogonia via lysine 48-linked polyubiquitination-mediated degradation of KRT36/KRT84. FASEB J 2023; 37: e23217.
[19] Zheng B, Zhao D, Zhang P, Shen C, Guo Y, Zhou T, Guo X, Zhou Z and Sha J. Quantitative proteomics reveals the essential roles of stromal interaction molecule 1 (STIM1) in the testicular cord formation in mouse testis. Mol Cell Proteomics 2015; 14: 2682-2691.
[20] Shen C, Yu J, Zhang X, Liu CC, Guo YS, Zhu JW, Zhang K, Yu Y, Gao TT, Yang SM, Li H, Zheng B and Huang XY. Strawberry notch 1 (SBNO1) promotes proliferation of spermatogonial stem cells via the noncanonical Wnt pathway in mice. Asian J Androl 2019; 21: 345-350.
[21] Xu W, Wang J, Xu J, Li S, Zhang R, Shen C, Xie M, Zheng B and Gu M. Long non-coding RNA DEPDC1-AS1 promotes proliferation and mi-

gration of human gastric cancer cells HGC-27 via the human antigen R-F11R pathway. J Int Med Res 2022; 50: 3000605221093135.
[22] Xue J, Wu T, Huang C, Shu M, Shen C, Zheng B and Lv J. Identification of proline-rich protein 11 as a major regulator in mouse spermatogonia maintenance via an increase in BMI1 protein stability. Mol Biol Rep 2022; 49: 9555-9564.
[23] Liu JY, Jiang YN, Huang H, Xu JF, Wu YH, Wang Q, Zhu Y, Zheng B, Shen C, Qian WF and Shen J. BMI-1 promotes breast cancer proliferation and metastasis through different mechanisms in different subtypes. Cancer Sci 2023; 114: 449-462.
[24] Xu BY, Yu XL, Gao WX, Gao TT, Hu HY, Wu TT, Shen C, Huang XY, Zheng B and Wu YB. RNF187 governs the maintenance of mouse GC-2 cell development by facilitating histone H3 ubiquitination at K57/80. Asian J Androl 2024; 26: 272-281.
[25] Shen C, Cao R, Zhou Q, Zhou T, Wu T, Gao W, Wang G, Feng G, Qiao L and Wang T. LINC00654 promotes ovarian cancer progression by facilitating nuclear export of HuR and stabilizing oncogenic mRNAs. Oncogene 2025; 44: 3422-3436.
[26] Liu M, Gao W, Sheng W, Zhou N, Wu T, Shen C, Feng G and Xi X. Dcun1d3 is dispensable for spermatogenesis and male fertility in mice. Am J Clin Exp Immunol 2025; 14: 127-137.
[27] Chen L, Peters JE, Prins B, Persyn E, Traylor M, Surendran P, Karthikeyan S, Yonova-Doing E, Di Angelantonio E, Roberts DJ, Watkins NA, Ouwehand WH, Danesh J, Lewis CM, Bronson PG, Markus HS, Burgess S, Butterworth AS and Howson JMM. Systematic Mendelian randomization using the human plasma proteome to discover potential therapeutic targets for stroke. Nat Commun 2022; 13: 6143.
[28] Mishra A, Malik R, Hachiya T, Jürgenson T, Namba S, Posner DC, Kamanu FK, Koido M, Le Grand Q, Shi M, He Y, Georgakis MK, Caro I, Krebs K, Liaw YC, Vaura FC, Lin K, Winsvold BS, Srinivasasainagendra V, Parodi L, Bae HJ, Chauhan G, Chong MR, Tomppo L, Akinyemi R, Roshchupkin GV, Habib N, Jee YH, Thomassen JQ, Abedi V, Cárcel-Márquez J, Nygaard M, Leonard HL, Yang C, Yonova-Doing E, Knol MJ, Lewis AJ, Judy RL, Ago T, Amouyel P, Armstrong ND, Bakker MK, Bartz TM, Bennett DA, Bis JC, Bordes C, Børte S, Cain A, Ridker PM, Cho K, Chen Z, Cruchaga C, Cole JW, de Jager PL, de Cid R, Endres M, Ferreira LE, Geerlings MI, Gasca NC, Gudnason V, Hata J, He J, Heath AK, Ho YL, Havulinna AS, Hopewell JC, Hyacinth HI, Inouye M, Jacob MA, Jeon CE, Jern C, Kamouchi M, Keene KL, Kitazono T, Kittner SJ, Konuma T, Kumar A, Lacaze P, Launer LJ, Lee KJ, Lepik K, Li J, Li L, Manichaikul A, Markus HS, Marston NA, Meitinger T, Mitchell BD, Montellano FA, Morisaki T, Mosley TH, Nalls MA, Nordestgaard BG, O'Donnell MJ, Okada Y, Onland-Moret NC, Ovbiagele B, Peters A, Psaty BM, Rich SS, Rosand J, Sabatine MS, Sacco RL, Saleheen D, Sandset EC, Salomaa V, Sargurupremraj M, Sasaki M, Satizabal CL, Schmidt CO, Shimizu A, Smith NL, Sloane KL, Sutoh Y, Sun YV, Tanno K, Tiedt S, Tatlisumak T, Torres-Aguila NP, Tiwari HK, Trégouët DA, Trompet S, Tuladhar AM, Tybjærg-Hansen A, van Vugt M, Vibo R, Verma SS, Wiggins KL, Wennberg P, Woo D, Wilson PWF, Xu H, Yang Q, Yoon K, Millwood IY, Gieger C, Ninomiya T, Grabe HJ, Jukema JW, Rissanen IL, Strbian D, Kim YJ, Chen PH, Mayerhofer E, Howson JMM, Irvin MR, Adams H, Wassertheil-Smoller S, Christensen K, Ikram MA, Rundek T, Worrall BB, Lathrop GM, Riaz M, Simonsick EM, Kõrv J, França PHC, Zand R, Prasad K, Frikke-Schmidt R, de Leeuw FE, Liman T, Haeusler KG, Ruigrok YM, Heuschmann PU, Longstreth WT, Jung KJ, Bastarache L, Paré G, Damrauer SM, Chasman DI, Rotter JI, Anderson CD, Zwart JA, Niiranen TJ, Fornage M, Liaw YP, Seshadri S, Fernández-Cadenas I, Walters RG, Ruff CT, Owolabi MO, Huffman JE, Milani L, Kamatani Y, Dichgans M and Debette S. Stroke genetics informs drug discovery and risk prediction across ancestries. Nature 2022; 611: 115-123.
[29] Zheng Y, Ren Z, Liu Y, Yan J, Chen C, He Y, Shi Y, Cheng F, Wang Q, Li C and Wang X. T cell interactions with microglia in immune-inflammatory processes of ischemic stroke. Neural Regen Res 2025; 20: 1277-1292.
[30] Shi SX, Xiu Y, Li Y, Yuan M, Shi K, Liu Q, Wang X and Jin WN. CD4(+) T cells aggravate hemorrhagic brain injury. Sci Adv 2023; 9: eabq0712.
[31] Xie W, Simats A, Guo Y, Huang T, Sun X, Chen W, Lin Y, Wang X, Lai Z, Yu W, Liesz A and Li P. Perspective review of myeloid immune cell responses and poststroke immunosuppression. Stroke 2023; 54: 1920-1929.
[32] Liu Y, Chen S, Liu S, Wallace KL, Zille M, Zhang J, Wang J and Jiang C. T-cell receptor signaling modulated by the co-receptors: potential targets for stroke treatment. Pharmacol Res 2023; 192: 106797.
[33] Mo L, Pan W, Cao W, Wang K and Huang L. Immune cells and intracerebral hemorrhage: a causal investigation through Mendelian randomization. Brain Behav 2025; 15: e70263.
[34] Hayes CA, Wilson D, De Leon MA, Mustapha MJ, Morales S, Odden MC and Ashpole NM. Insulin-like growth factor-1 and cognitive health: exploring cellular, preclinical, and clinical dimensions. Front Neuroendocrinol 2025; 76: 101161.

[35] Arjunan A, Sah DK, Woo M and Song J. Identification of the molecular mechanism of insulin-like growth factor-1 (IGF-1): a promising therapeutic target for neurodegenerative diseases associated with metabolic syndrome. Cell Biosci 2023; 13: 16.

[36] Jiang Y, Liu Q, Wang C, Zhao Y, Jin C, Sun M and Ge S. The interplay between cytokines and stroke: a bi-directional Mendelian randomization study. Sci Rep 2024; 14: 17657.

[37] Mattson NM, Chan AKN, Miyashita K, Mukhaleva E, Chang WH, Yang L, Ma N, Wang Y, Pokharel SP, Li M, Liu Q, Xu X, Chen R, Singh P, Zhang L, Elsayed Z, Chen B, Keen D, Pirrotte P, Rosen ST, Chen J, LaBarge MA, Shively JE, Vaidehi N, Rockne RC, Feng M and Chen CW. A novel class of inhibitors that disrupts the stability of integrin heterodimers identified by CRISPR-tiling-instructed genetic screens. Nat Struct Mol Biol 2024; 31: 465-475.

[38] Lin X, Huang S, Gao S, Liu J, Tang J and Yu M. Integrin β5 subunit regulates hyperglycemia-induced vascular endothelial cell apoptosis through FoxO1-mediated macroautophagy. Chin Med J (Engl) 2024; 137: 565-576.

[39] Keith J, Christakopoulos GE, Fernandez AG, Yao Y, Zhang J, Mayberry K, Telange R, Sweileh RBA, Dudley M, Westbrook C, Sheppard H, Weiss MJ and Lechauve C. Loss of miR-144/451 alleviates β-thalassemia by stimulating ULK1-mediated autophagy of free α-globin. Blood 2023; 142: 918-932.

[40] Hao S, Luo J, Yuan S, Chen W, Zhang X, Zhao C, Xu H, Liu Z and Zhang D. The DRP1 inhibitory peptide P110 provides neuroprotection after subarachnoid hemorrhage by suppressing neuronal apoptosis and stabilizing the blood-brain barrier. Free Radic Biol Med 2025; 240: 1-14.

Table S1. Immune cell phenotypes included in the study

ID	Immune cell phenotypes	Panel	Trait type
GCST90002082	SSC-A on CD8br	TBNK	Morphological parameter
GCST90001940	CD25 on CD39+ activated Treg	Treg	MFI
GCST90002101	CD45RA on TD CD8br	Maturation stages of T cell	MFI
GCST90001418	CD24+ CD27+ AC	B cell	Absolute count
GCST90002115	HLA DR on HLA DR+ CD8br	TBNK	MFI
GCST90001406	Memory B cell %B cell	B cell	Relative count
GCST90001397	Unsw mem %B cell	B cell	Relative count
GCST90002032	CD39 on CD39+ CD4+	Treg	MFI
GCST90002106	HLA DR on DC	cDC	MFI
GCST90001704	BAFF-R on IgD+ CD24-	B cell	MFI
GCST90001864	CD3 on CD28+ CD45RA+ CD8br	Treg	MFI
GCST90001808	CD27 on sw mem	B cell	MFI
GCST90001681	CD25++ CD8br AC	Treg	Absolute count
GCST90001523	CD33- HLA DR+ AC	Myeloid cell	Absolute count
GCST90001575	Naive CD4+ %T cell	Maturation stages of T cell	Relative count
GCST90001663	CD28- CD8dim AC	Treg	Absolute count
GCST90001576	Transitional %B cell	B cell	Relative count
GCST90001490	CD39+ activated Treg %activated Treg	Treg	Relative count

TBNK, T cell-B cell-natural killer cell; Treg, regulatory T cell; cDC, conventional dendritic cell; MFI, median fluorescence intensity.

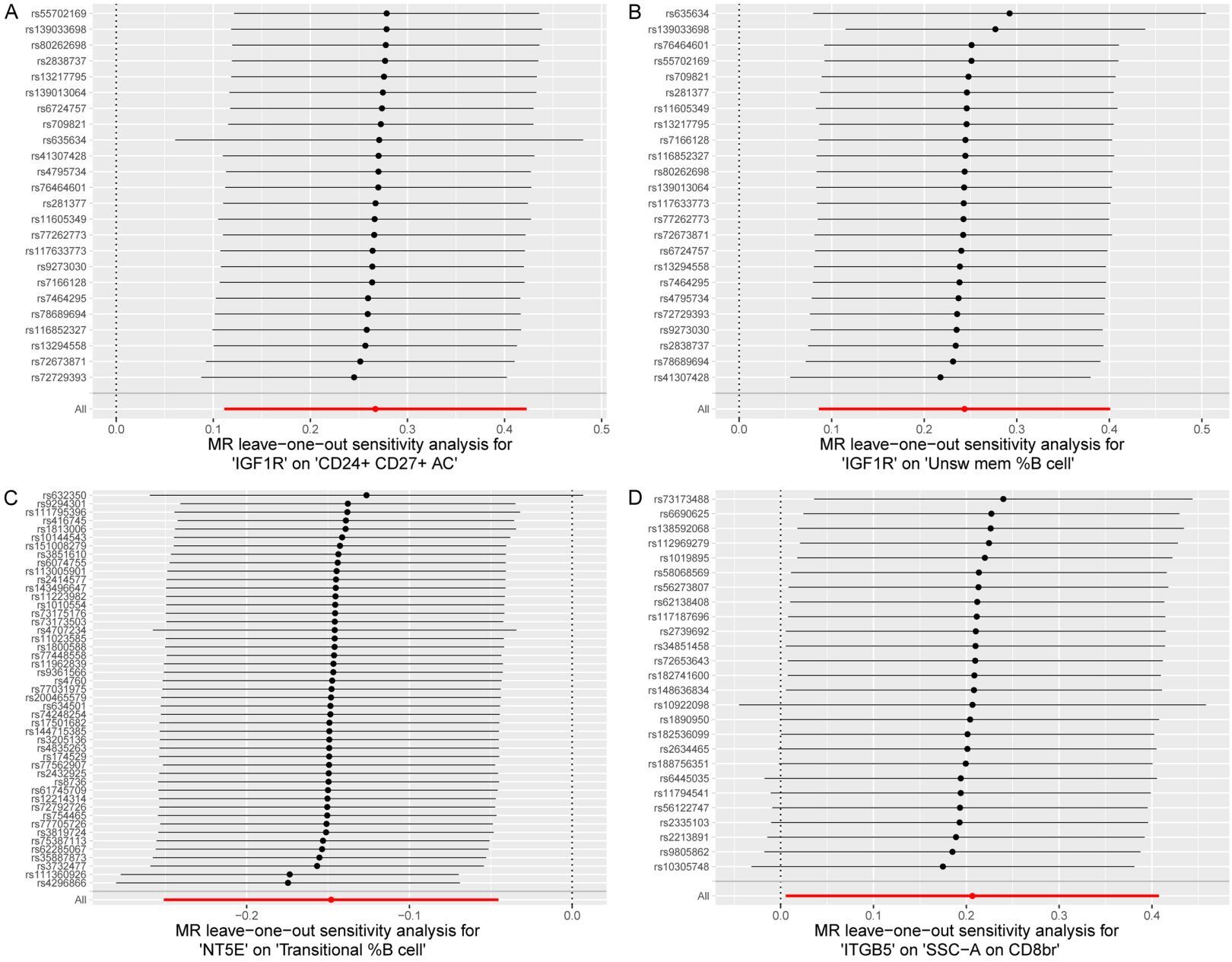
A
rs55702169
rs139033698
rs80262698
rs2838737
rs13217795
rs139013064
rs6724757
rs709821
rs635634
rs41307428
rs4795734
rs76464601
rs281377
rs11605349
rs77262773
rs117633773
rs9273030
rs7166128
rs7464295
rs78689694
rs116852327
rs13294558
rs72673871
rs72729393
All
0.0
0.1
0.2
0.3
0.4
0.5
MR leave−one−out sensitivity analysis for
'IGF1R' on 'CD24+ CD27+ AC'
B
rs635634
rs139033698
rs76464601
rs55702169
rs709821
rs281377
rs11605349
rs13217795
rs7166128
rs116852327
rs80262698
rs139013064
rs117633773
rs77262773
rs72673871
rs6724757
rs13294558
rs7464295
rs4795734
rs72729393
rs9273030
rs2838737
rs78689694
rs41307428
All
0.0
0.1
0.2
0.3
0.4
0.5
MR leave−one−out sensitivity analysis for
'IGF1R' on 'Unsw mem %B cell'
C
rs632350
rs9294301
rs111795396
rs4716745
rs1813006
rs10144543
rs151008279
rs3851610
rs6074755
rs113005901
rs2414577
rs143496647
rs11223982
rs1010554
rs73175176
rs73173503
rs4707234
rs11023585
rs1800588
rs77448558
rs11962839
rs9361566
rs4760
rs77031975
rs200465579
rs634501
rs74248254
rs17501682
rs144715385
rs3205136
rs4835263
rs174529
rs77562907
rs2432925
rs8736
rs61745709
rs12214314
rs72792726
rs754465
rs77705726
rs3819724
rs75387113
rs62285067
rs35887873
rs3732477
rs111360926
rs4296866
All
−0.2
−0.1
0.0
MR leave−one−out sensitivity analysis for
'NT5E' on 'Transitional %B cell'
D
rs73173488
rs6690625
rs138592068
rs112969279
rs1019895
rs58068569
rs56273807
rs62138408
rs117187696
rs2739692
rs34851458
rs72653643
rs182741600
rs148636834
rs10922098
rs1890950
rs182536099
rs2634465
rs188756351
rs6445035
rs11794541
rs56122747
rs2335103
rs2213891
rs9805862
rs10305748
All
0.0
0.1
0.2
0.3
0.4
MR leave−one−out sensitivity analysis for
'ITGB5' on 'SSC−A on CD8br'

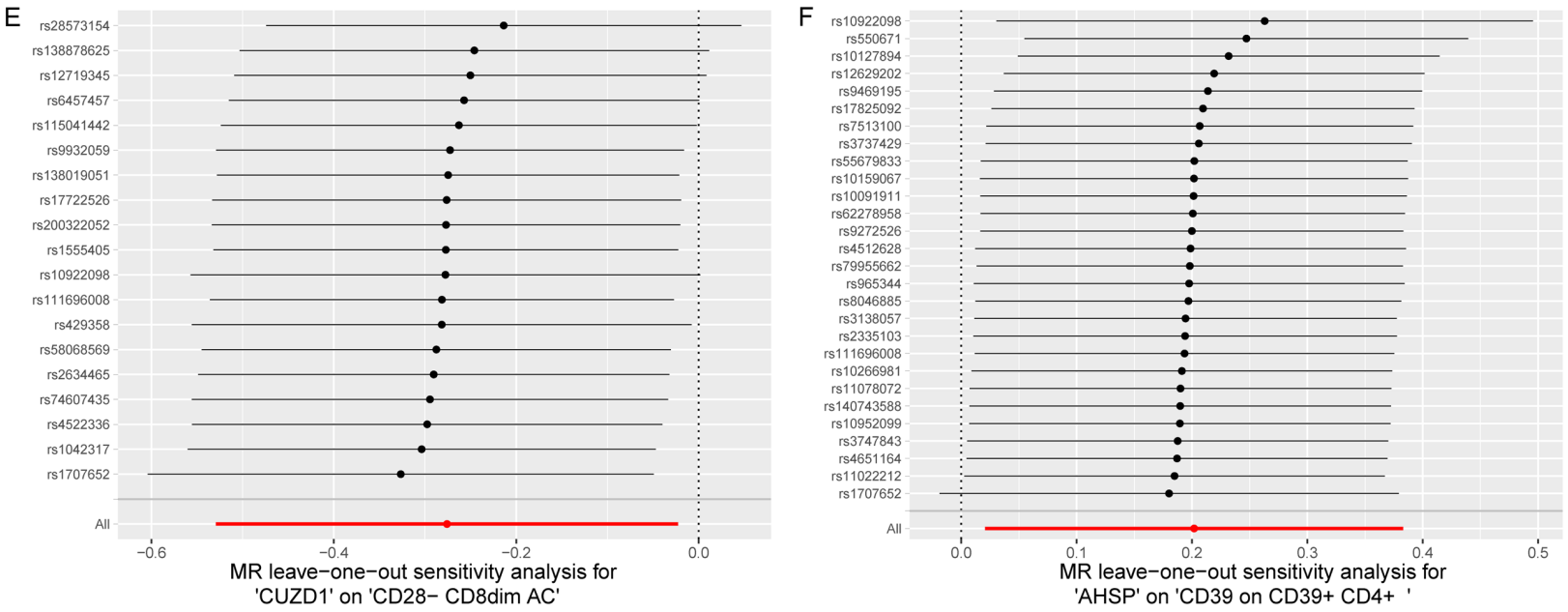

Figure S1. Leave-one-out analysis of Mendelian randomization (MR) for plasma proteins and immune cell phenotypes. A. Leave-one-out analysis of MR for IGF1R on CD24+ CD27+ AC. B. Leave-one-out analysis of MR for IGF1R on Unsw mem %B cell. C. Leave-one-out analysis of MR for NT5E on Transitional %B cell. D. Leave-one-out analysis of MR for ITGB5 on SSC-A on CD8br. E. Leave-one-out analysis of MR for CUZD1 on CD28- CD8dim AC. F. Leave-one-out analysis of MR for AHSP on CD39 on CD39+ CD4+.

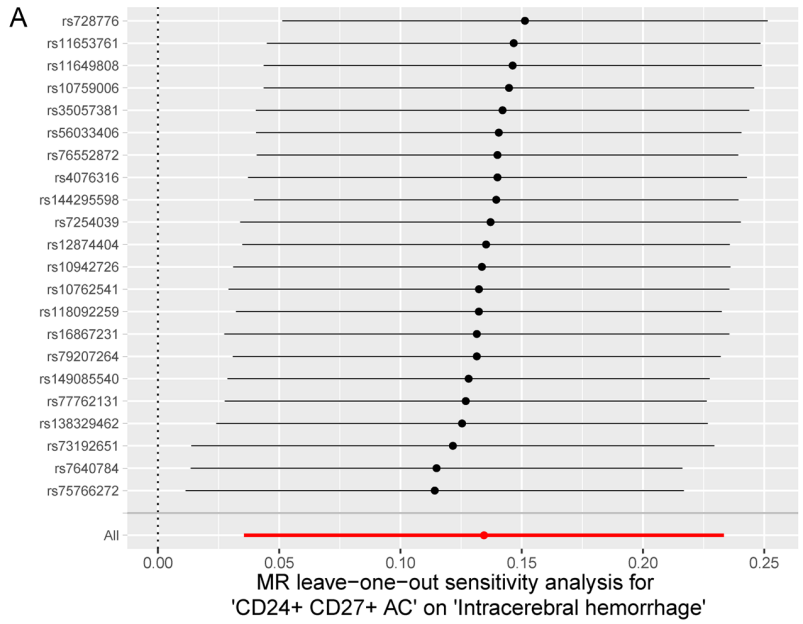
A
rs728776
rs11653761
rs11649808
rs10759006
rs35057381
rs56033406
rs76552872
rs4076316
rs144295598
rs7254039
rs12874404
rs10942726
rs10762541
rs118092259
rs16867231
rs79207264
rs149085540
rs77762131
rs138329462
rs73192651
rs7640784
rs75766272
All
0.00
0.05
0.10
0.15
0.20
0.25
MR leave−one−out sensitivity analysis for
'CD24+ CD27+ AC' on 'Intracerebral hemorrhage'

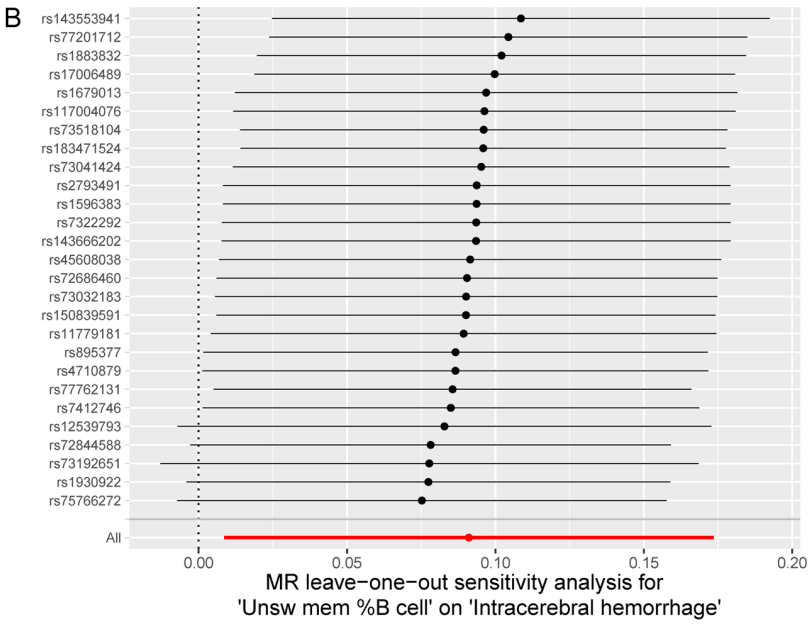
B
rs143553941
rs77201712
rs1883832
rs17006489
rs1679013
rs117004076
rs73518104
rs183471524
rs73041424
rs2793491
rs1596383
rs7322292
rs143666202
rs45608038
rs72686460
rs73032183
rs150839591
rs11779181
rs895377
rs4710879
rs77762131
rs7412746
rs12539793
rs72844588
rs73192651
rs1930922
rs75766272
All
0.00
0.05
0.10
0.15
0.20
MR leave−one−out sensitivity analysis for
'Unsw mem %B cell' on 'Intracerebral hemorrhage'

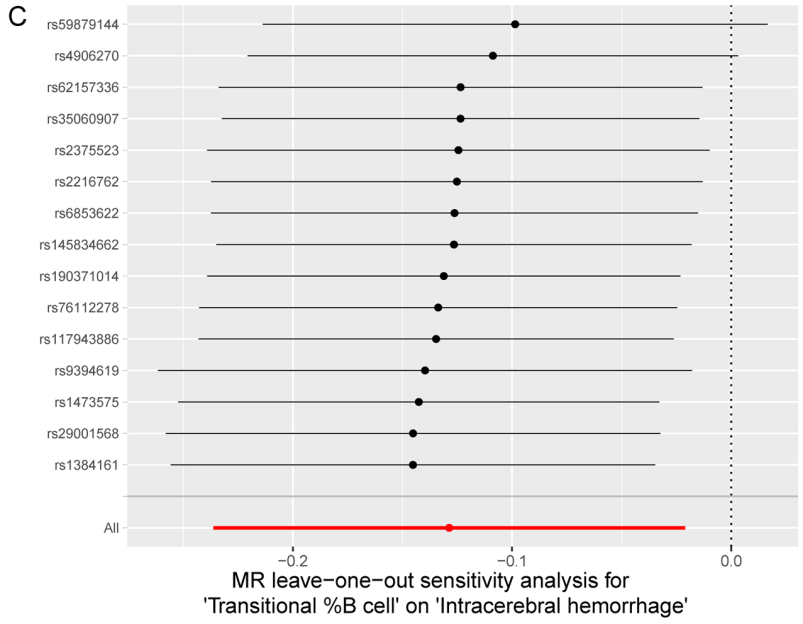
C
rs59879144
rs4906270
rs62157336
rs35060907
rs2375523
rs2216762
rs6853622
rs145834662
rs190371014
rs76112278
rs117943886
rs9394619
rs1473575
rs29001568
rs1384161
All
−0.2
−0.1
0.0
MR leave−one−out sensitivity analysis for
'Transitional %B cell' on 'Intracerebral hemorrhage'

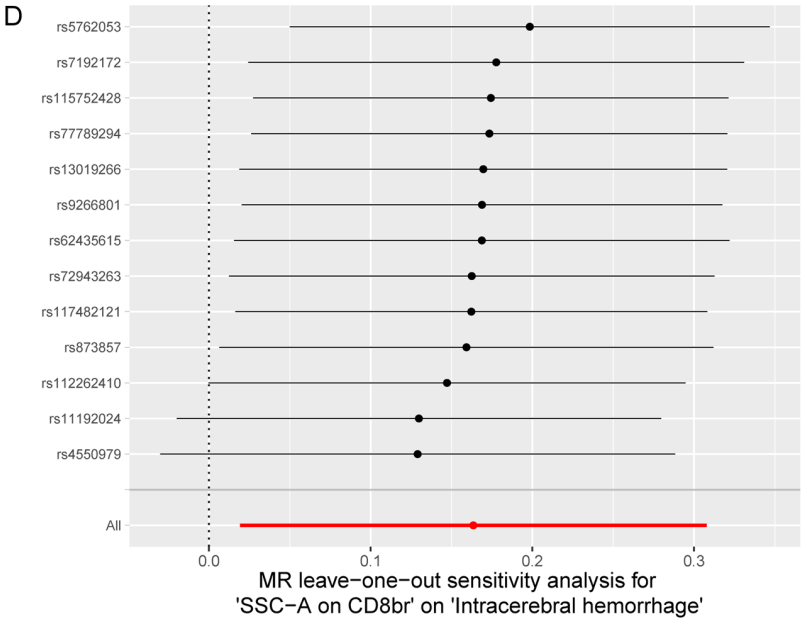
D
rs5762053
rs7192172
rs115752428
rs77789294
rs13019266
rs9266801
rs62435615
rs72943263
rs117482121
rs873857
rs112262410
rs11192024
rs4550979
All
0.0
0.1
0.2
0.3
MR leave−one−out sensitivity analysis for
'SSC−A on CD8br' on 'Intracerebral hemorrhage'

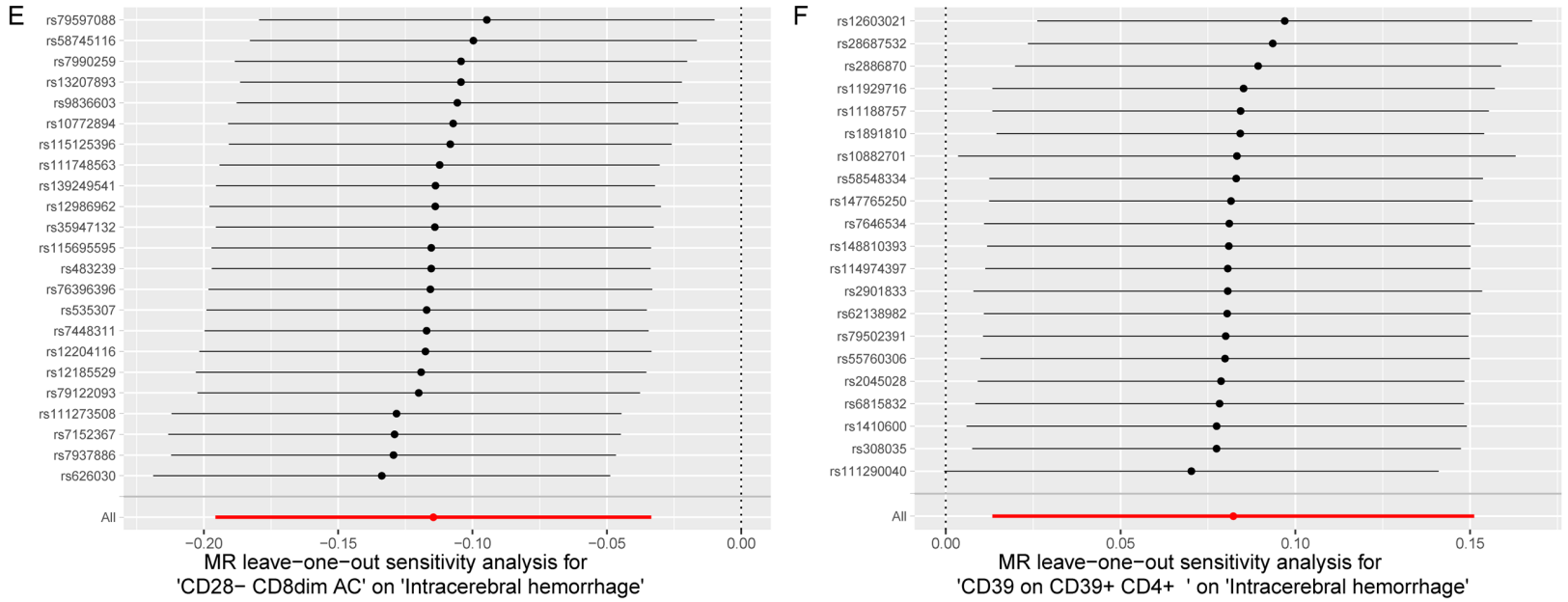

Figure S2. Leave-one-out analysis of MR for immune cell phenotypes and intracerebral hemorrhage (ICH). A. Leave-one-out analysis of MR for CD24+ CD27+ AC on ICH. B. Leave-one-out analysis of MR for Unsw mem %B cell on ICH. C. Leave-one-out analysis of MR for Transitional %B cell on ICH. D. Leave-one-out analysis of MR for SSC-A on CD8br on ICH. E. Leave-one-out analysis of MR for CD28- CD8dim AC on ICH. F. Leave-one-out analysis of MR for CD39 on CD39+ CD4+ on ICH.

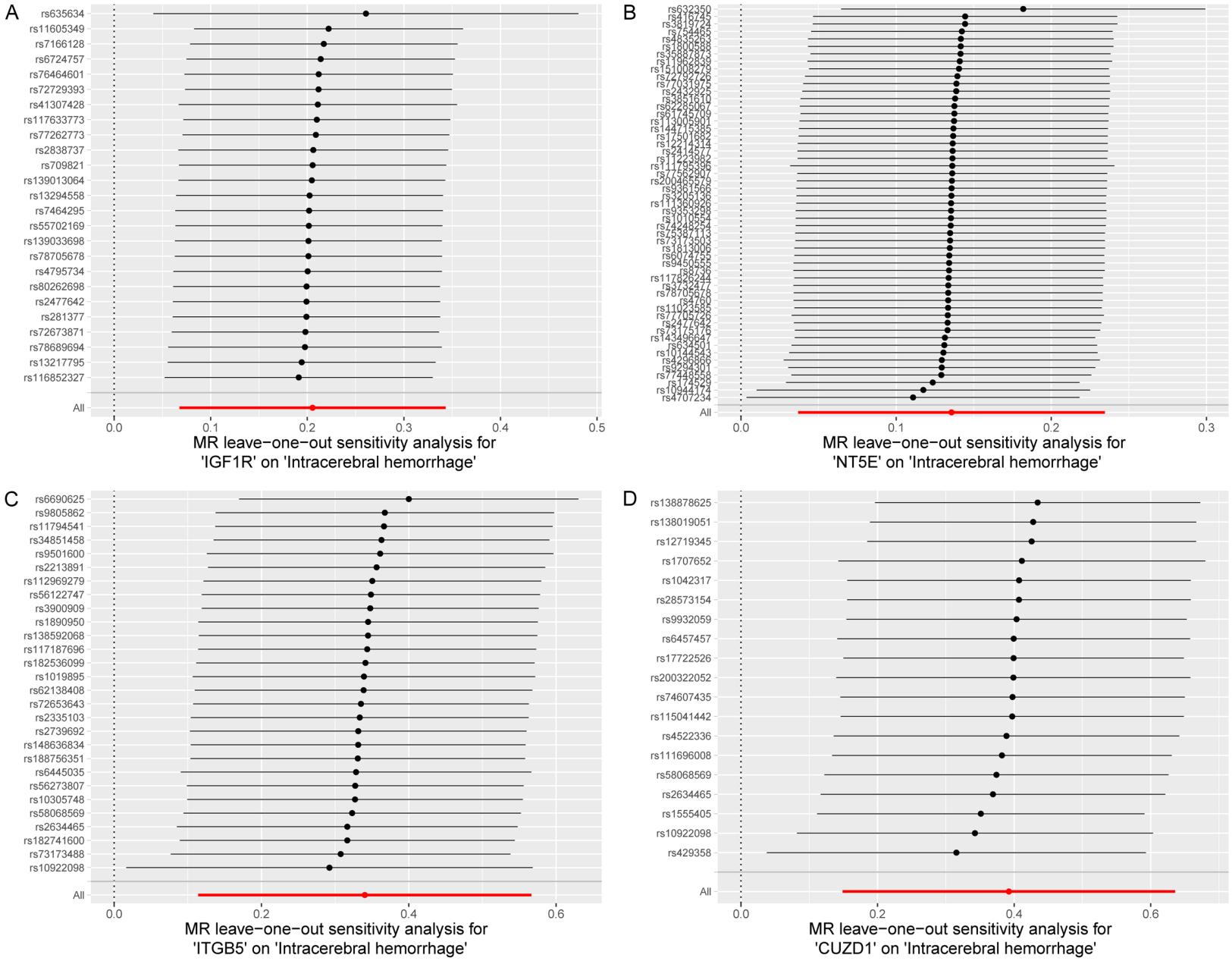
A
rs635634
rs11605349
rs7166128
rs6724757
rs76464601
rs72729393
rs41307428
rs117633773
rs77262773
rs2838737
rs709821
rs139013064
rs13294558
rs7464295
rs55702169
rs139033698
rs78705678
rs4795734
rs80262698
rs2477642
rs281377
rs72673871
rs78689694
rs13217795
rs116852327
All
0.0
0.1
0.2
0.3
0.4
0.5
MR leave−one−out sensitivity analysis for
'IGF1R' on 'Intracerebral hemorrhage'
B
All
0.0
0.1
0.2
0.3
MR leave−one−out sensitivity analysis for
'NT5E' on 'Intracerebral hemorrhage'
C
rs6690625
rs9805862
rs11794541
rs34851458
rs9501600
rs2213891
rs112969279
rs56122747
rs3900909
rs1890950
rs138592068
rs117187696
rs182536099
rs1019895
rs62138408
rs72653643
rs2335103
rs2739692
rs148636834
rs188756351
rs6445035
rs56273807
rs10305748
rs58068569
rs2634465
rs182741600
rs73173488
rs10922098
All
0.0
0.2
0.4
0.6
MR leave−one−out sensitivity analysis for
'ITGB5' on 'Intracerebral hemorrhage'
D
rs138878625
rs138019051
rs12719345
rs1707652
rs1042317
rs28573154
rs9932059
rs6457457
rs17722526
rs200322052
rs74607435
rs115041442
rs4522336
rs111696008
rs58068569
rs2634465
rs1555405
rs10922098
rs429358
All
0.0
0.2
0.4
0.6
MR leave−one−out sensitivity analysis for
'CUZD1' on 'Intracerebral hemorrhage'

E

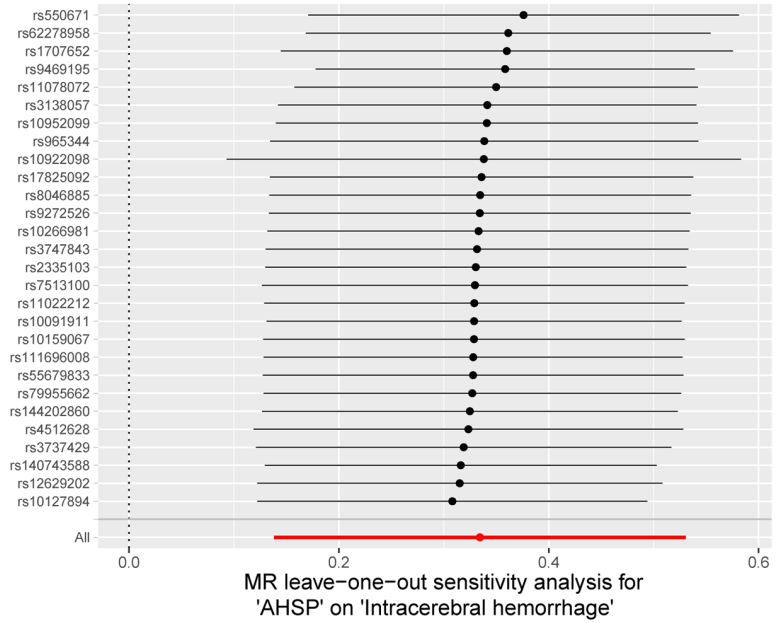

Figure S3. Leave-one-out analysis of MR for plasma proteins and ICH. A. Leave-one-out analysis of MR for IGF1R on ICH. B. Leave-one-out analysis of MR for NT5E on ICH. C. Leave-one-out analysis of MR for ITGB5 on ICH. D. Leave-one-out analysis of MR for CUZD1 on ICH. E. Leave-one-out analysis of MR for AHSP on ICH.